ADVANCED MATERIALS
www.advmat.de

www.MaterialsViews.com

A Hyper-Stretchable Elastic-Composite Energy Harvester

Chang Kyu Jeong, Jinhwan Lee, Seungyong Han, Jungho Ryu, Geon-Tae Hwang, Dae Yong Park, Jung Hwan Park, Seung Seob Lee, Myunghwan Byun, Seung Hwan Ko, and Keon Jae Lee**

Stretchable electronics that offer elastic characteristics in response to large strain deformation have attracted significant interest for use in a number of new applications, such as artificial electronic skins (e-skins),[1–4] epidermal/biomedical devices,[5,6] biomimetic lenses,[7] and body sensor networks (BSNs).[8] Although diverse approaches have been attempted to develop practical stretchable/wearable electronics and batteries,[9–11] a challenging problem is in power supplies, which should have similar elastic properties to achieve their co-integration with stretchable devices. Consequently, the stretchability of high-output energy-conversion devices is a critical hurdle to their direct and conformal assembly in stretchable electronic systems for operating various consumer products. In this regard, flexible piezoelectric energy harvesters, called nanogenerators, have attracted remarkable attention due to the capability of generating/collecting energy in mechanical strain-driven occasions of ambient surroundings and biological bodies.[12–17] Recently, high-performance flexible nanogenerators have been demonstrated using perovskite thin films such as $BaTiO_3$,[18] $PbZr_xTi_{1-x}O_3$ (PZT),[19,20] and $(1-x)\{Pb(Mg_{1/3}Nb_{2/3})O_3\}-x\{PbTiO_3\}$ (lead magnesio niobate–lead titanate) (PMN-PT),[21] even for milliwatt-scale energy harvesting. It is noteworthy that these novel piezoelectric generators can be employed to realize self-powered flexible electronic systems,[22,23] biomedical stimulators,[21] implantable devices,[19,24] and biomimetic acoustic nanosensors.[25,26] Another approach is the nanocomposite generator (NCG), which can provide cost-effective and large-area energy harvesting without any vacuum process.[27–32] Although NCGs have been regarded as a concept of stretchy piezoelectric systems, the authentically operating stretchable NCG has not been yet realized due to the absence of proper stretchable electrodes and robust composite matrix.[33–35] While these bendable nanogenerators have been intensively studied using diverse piezoelectric materials and structures, the development of stretchable high-output energy harvesters still requires further investigation to realize self-powered stretchable electronic systems.

Several researchers have explored buckling structures with piezoelectric ribbons[36–38] or micropatterning-notched structures with polyvinylidenefloride (PVDF)/graphene.[39] They reported producing output currents of tens of picoamperes to nanoamperes with the elongating/releasing stretchable energy harvesters. However, the generated output was insufficient to operate practical electronic devices, due to the narrow/confined piezoactive ribbons or the low piezoelectricity. In addition, the stretchable energy harvesters suffer from deficient stretchability (below a few tens of percentage) and poor reversibility caused by intrinsic material stiffness and structural dependency, resulting in unstable output signals, incompatible integration, and limited mechanical durability. To achieve ideal stretchable nanogenerators, a new concept is needed for resolving critical issues that incorporate highly elastic piezoelectric components with high-output performance and co-assembly with ultra-stretchable electrodes.

Herein, we demonstrate a simple and facile route to a high-performance and hyper-stretchable elastic-composite generator (SEG) realized by very long Ag nanowires (VAgNWs) stretchable electrodes. This stretchable energy harvester exhibits over ten times larger stretchability (≈200%) and about seven times higher power output (≈4 V and ≈500 nA), compared to the previous stretchable piezo-nanogenerator. The outstanding performance was achieved by employing a rubber-based piezoelectric elastic composite (PEC) and the very long nanowire percolation (VLNP) electrodes, obviating device structural dependency. The remarkable elongation rate of the reinforced rubbery matrix mechanically stimulates the imbedded piezoelectric particles to efficiently induce piezopotential throughout the entire PEC. To demonstrate the stable and conformal integration of the SEG with highly stretchable VLNP electrodes, the VAgNWs were successfully transferred onto the surfaces of PEC composed of PMN-PT particles and multiwalled carbon nanotubes (MWCNTs) in a silicone elastomer matrix. The principles of robust stretchability and well-distributed piezopotential generation were also simulated using finite element analysis (FEA) to investigate the notable stress relaxation of VLNP over short NWs. Our SEG can directly produce electrical

C. K. Jeong, G.-T. Hwang, D. Y. Park, J. H. Park, Dr. M. Byun, Prof. K. J. Lee
Department of Materials Science and Engineering
Korea Advanced Institute of Science and Technology (KAIST)
291 Daehak-ro, Yuseong-gu, Daejeon 305-701, South Korea
E-mail: keonlee@kaist.ac.kr

Dr. J. Lee, Dr. S. Han, Prof. S. H. Ko
Department of Mechanical Engineering
Seoul National University
1 Gwanak-ro, Gwanak-gu, Seoul 151-742, South Korea
E-mail: maxko@snu.ac.kr

Dr. J. Lee, Prof. S. S. Lee
Department of Mechanical Engineering
Korea Advanced Institute of Science and Technology (KAIST)
291 Daehak-ro, Yuseong-gu, Daejeon 305-701, South Korea

Dr. J. Ryu
Functional Ceramic Group
Korea Institute of Materials Science (KIMS)
797 Changwon-daero
Seongsan-gu
Changwon, Gyeongsangnam-do 642–831, South Korea

DOI: 10.1002/adma.201500367

energy by harnessing various mechanical stimuli (e.g., twisting, folding, crumpling, pressing), and can operate commercial electronic devices by stretching motions. Finally, wearable energy-harvesting clothes for highly stretchable stockings using the SEG were demonstrated in order to convert biomechanical-stretching energy to electricity.

Figure 1a illustrates the representative schematics of the SEG structure, composed of the hyper-stretchable PEC and VLNP electrodes. Ecoflex silicone rubber, selected as a starting material for the matrix of the PEC, is known as an ultra-stretchable elastomer which can be theoretically elongated up to ≈900% in elastic deformation without mechanical breakage, which is overwhelmingly superior to polydimethylsiloxane (PDMS) matrix (<100% in plastic deformation). A well-granulated mixture of PMN-PT particles and MWCNTs was blended and dispersed in the silicone rubber prepolymer. The weight composition of the piezoelectric mixture was optimized to be 20% in the rubbery matrix because this weight percentage of composite was the maximum amount for good molding. After curing and demolding the PEC, the VAgNWs synthesized by the successive multistep growth (SMG) method were filtered by a suction pressure process, and stably transferred onto both sides of the PEC (Figure 1a(i)). The VAgNWs can achieve a highly percolated network nanostructure, which serves as a stretchable electrode with high conductivity and stability.[40] Subsequent thermal annealing at 200 °C was performed to allow nanowelding between the VAgNWs to ensure low electrical resistance; note that the polyvinylpyrrolidone (PVP) surfactant was also removed during this thermal treatment. To align ferroelectric dipoles in the PMN-PT particles, a poling process was conducted with an external voltage of 50 kV cm^{-1} at 110 °C, followed by metal cable or plate wiring. The polarization ensures that the dipoles in the PMN-PT microparticles are arranged along the electric field direction, which is normal to the two parallel VLNP electrodes. Finally, a hyper-stretchable and elastic energy harvester was fabricated to produce electricity (Figure 1a(ii)). The bottom panels in Figure 1a are magnified illustrations of the VLNP electrode on the PEC. When the PEC is stretched by external force, the piezoelectric particles in the matrix can be stressed by the mechanical strain which causes a variation of piezoelectric dipoles (ΔP) in the PEC. The change of dipole moments causes the VLNP electrodes accumulate or push electrons through an outer load, generating output electricity (the bottom of Figure 1a(ii)). The detailed fabrication, optimization, and circuital mechanism are described in Figure S1 in the Supporting Information.

As shown in Figure 1b, the SEG, consisting of both a highly elastic silicone-rubbery matrix and long NW percolated network electrodes, showed excellent stretchability above 200% without any mechanical cracking or delamination of the VLNP electrodes. The stretchable VLNP electrode (below 10 Ω sq^{-1}) was formed as a uniform, conformal, and dense film of percolated AgNWs, which guarantees a large portion of piezoactive area on the PEC, similar to conventional metal electrodes. Figure 1c presents a scanning electron microscopy (SEM) image of the PMN-PT microparticles and MWCNTs well dispersed in the PEC. During the granulating and mixing process, the ≈1 μm PMN-PT particles were closely entangled with MWCNTs (diameter of ≈20 nm and length of ≈10 μm). The MWCNTs act as physically dispersing, mechanically reinforcing, and electrically bridging agents in the piezoelectric composite, as previously reported.[27–29] Figure 1d shows an SEM image of uniformly sized PMN-PT microparticles prepared by the columbite precursor method[41] (Supporting Information, Figure S2) with the chemical composition of 0.65PMN-0.35PT, which is the morphotropic phase boundary (MPB) stoichiometry exhibiting exceedingly high piezoelectric coefficient (d_{33}) and electromechanical coupling factor (k_{33}) even in polycrystalline structures ($d_{33} \approx 690$ pC N^{-1} and $k_{33} \approx 0.73$) due to the excellent original properties of the single crystalline state ($d_{33} > 1200$ pC N^{-1} and $k_{33} > 0.9$).[42,43] X-ray diffraction (XRD) patterns of the PMN-PT particles indicate the perovskite crystal structure without any secondary byproduct crystal (inset of Figure 1d). To investigate the crystalline phase of the PMN-PT microparticles, we also performed Raman spectroscopy (Figure 1e). The Raman spectrum in a frequency range of 700–900 cm^{-1} (A_{1g} mode) can be deconvoluted into two envelopes at around 740 and 800 cm^{-1}, which indicate tetragonal symmetry (*P*4*mm*) and rhombohedral symmetry (*R*3*m*), respectively. This means the coexistence of two different symmetrical phases, *P*4*mm* and *R*3*m*, in the PMT-PT system with MPB composition. The dominant phase in our PMN-PT microparticles is tetragonal rather than rhombohedral (i.e., peak intensity at 740 cm^{-1} is slightly higher than that of 800 cm^{-1}), which is in good agreement with the previous reports for high piezoelectricity.[44] In addition, the aforementioned doublet bands manifest the presence of Ti–O bonds added to PMN, thus proving the PMN-PT is a complete solid solution without segregation of individual PMN and PT.[42]

The length of the AgNWs in the conductive NW percolation network is crucial for achieving robust electrical conductivity and mechanical stability.[40] Unfortunately, most of the geometric features of the metallic NWs chemically synthesized were restricted to 1–20 μm in length and displayed relatively weak electrical/mechanical properties.[45,46] To boost the length of AgNWs, we developed a novel SMG synthesis method (Supporting Information), which is beneficial for synthesizing VAgNWs with maximum length up to 500 μm (average length of 150 μm), as shown in Figure 1f and Figure S3 in the Supporting Information.[40] Our VAgNWs are extraordinarily long compared to typical AgNWs synthesized by the conventional polyol process.[47] In the SMG process, the width of the AgNWs remains about 100–150 nm (insets of Figure 1f,g), while the length grows continuously up to sub-millimeter scale, as demonstrated in our previous reports.[40,48,49] The high-resolution transmission electron microscopy (HRTEM) image in Figure 1g presents that the lengthwise lattice distance of VAgNW is about 1.45 Å and the growth direction is $[0\,2\,\bar{2}]$ of the AgNW's face-centered-cubic (FCC) structure, which is in good accords with the previous studies. As shown in the inset of Figure 1g, an HRSEM describes the pentagonal multi-twinned shape of the VAgNW, which is known to have high elasticity and yield strength, caused by the improved stiffness even compared to bulk Ag because of the internal twin boundaries of the NWs.[50,51]

The VLNP electrode is suitable for stretchable devices due to the effects of the long NW network and nanowelding.[40] A percolated network composed of long NWs can be more easily elongated and stretched than that of short NWs, as demonstrated

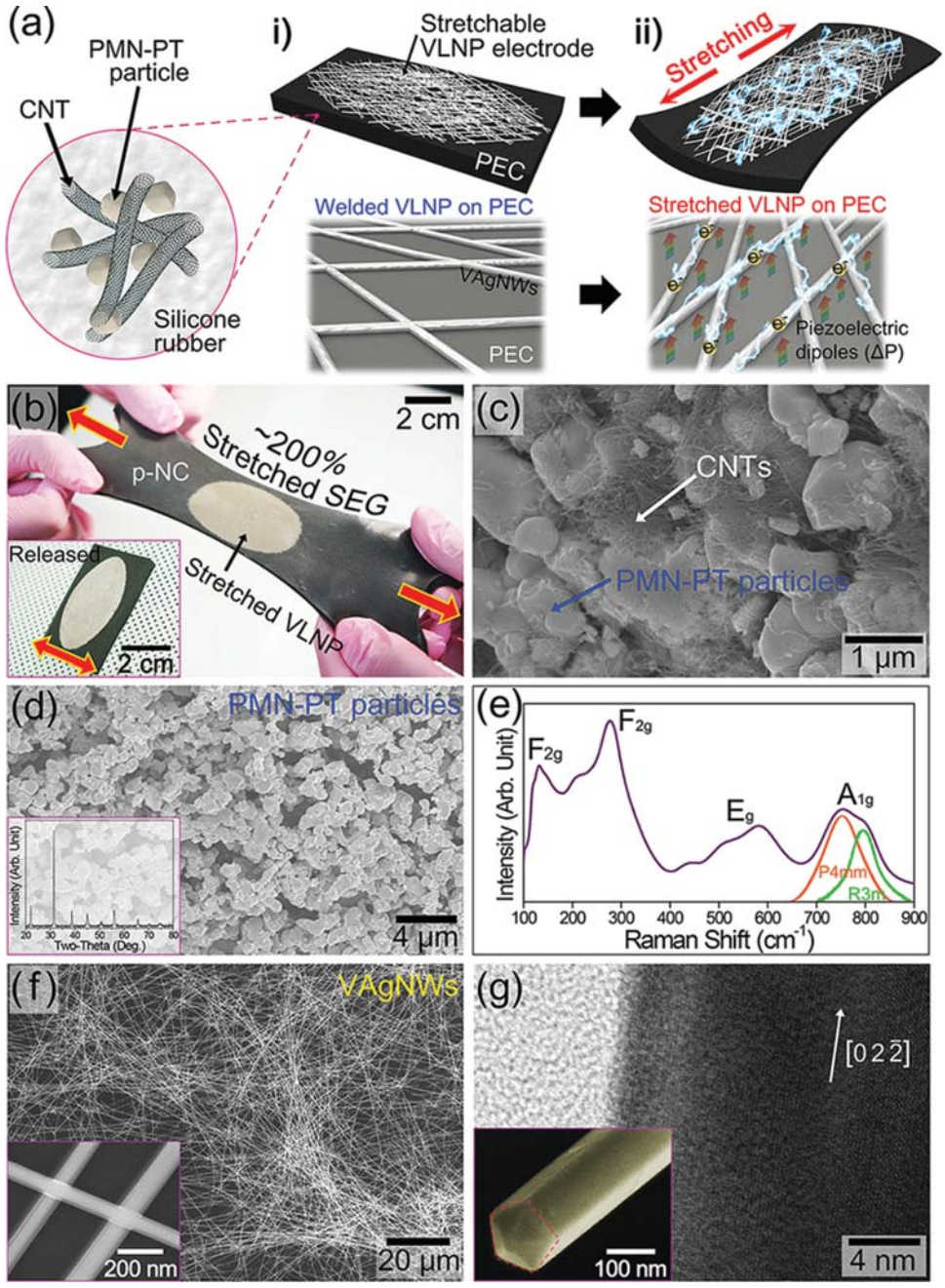

Figure 1. a) Schematic illustration of the hyper-stretchable and deformable nanocomposite generator. i) To fabricate stretchable VLNP electrodes, VAgNWs are transferred onto both sides of PEC composed of PMN-PT particles, MWCNTs, and silicone rubber matrix. ii) The SEG can generate electricity when it is stretched or deformed. The bottom panels illustrate the magnified schematics of stretchable VLNP electrode. The stretching motion of PEC can induce the change of piezoelectric dipoles (ΔP, denoted by the color-gradient arrow) in PMN-PT particles, which makes electric potential and electron flows through the VAgNWs of VLNP electrodes. b) The final SEG device stretched by human hands. The inset shows the SEG is released again without damage. c) An SEM image of the well-dispersed nanomaterials consisting of PMN-PT microparticles and MWCNTs. d) An SEM micrograph showing the uniform-sized PMN-PT microparticles synthesized by the columbite precursor method. The inset is the XRD patterns of the PMN-PT particles. e) A high-resolution dispersive Raman spectrum of the PMN-PT particles, which presents perovskite crystalline structure with the MPB composition has two crystal symmetry, *P4mm* and *R3m*. f) Overall and magnified (inset) SEM pictures of VAgNWs synthesized by the successive multistep growth (SMG) method. g) An HRTEM image of VAgNW with the growth direction of [02$\bar{2}$]. Inset: An HRSEM image of VAgNW indicating the pentagonal multi-twinned structure (red dashed line).

in the numerical FEA simulation (**Figure 2**a(i)). The simulation result also shows that the percolation network of longer NWs undergoes smaller maximum stress, compared to that of shorter NWs under the same strain condition (Figure 2a(ii)). In other words, the more junctions of the shorter NW mesh make the percolation network stiffer and denser, which cannot

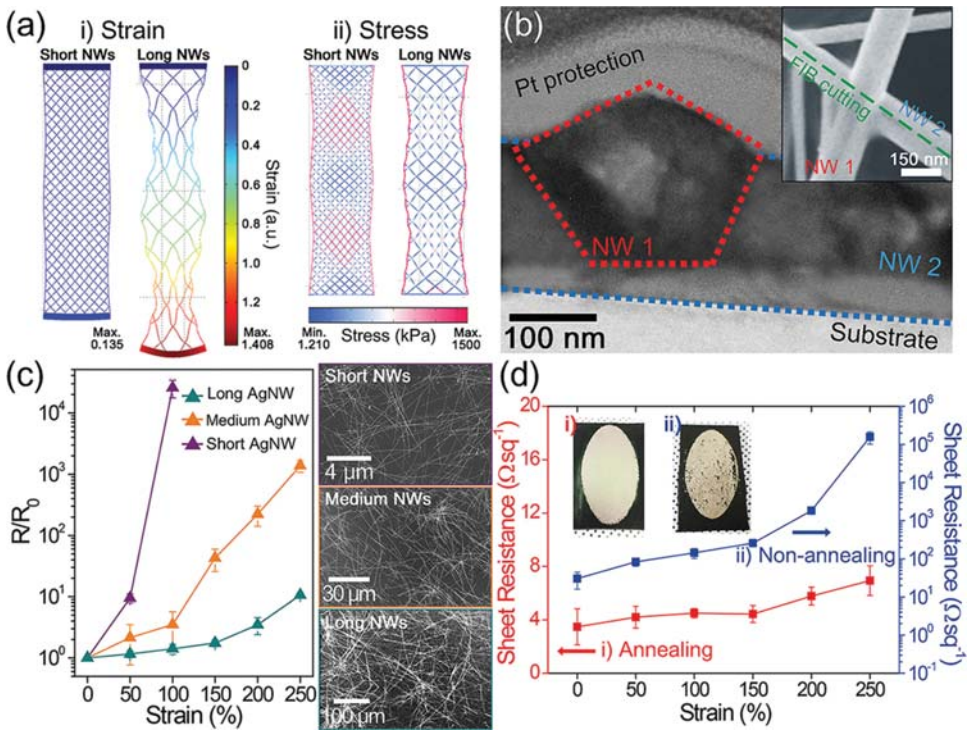

Figure 2. a) COMSOL simulations of structural mechanics about deformed NW networks according to the length of NWs. i) The degree of strain in short and long NW networks under same stress. ii) The stress distribution in short and long NW networks under same strain. The highly stressed left and right edges are just for establishment of finite element modeling, not for network structures. b) TEM image of the two crossing VAgNWs at the junction as shown in the inset SEM image. The nanowelded NW pair was processed by focused ion beam (FIB) for the analysis. c) The relative resistance change of short NW (purple), medium NW (orange), and very long NW (turquoise) percolation network electrodes during stretching motions. The right panels are SEM images of each NW. The magnified SEM of VAgNWs is shown in Figure S3 in the Supporting Information. d) Under increasing strain, the sheet resistance changes of stretchable VLNP electrodes with (i) and without (ii) annealing which can induce nanowelding of VAgNWs. The insets show digital photographs of SEG devices after stretching tests.

accommodate non-destructive stress relaxation. In contrast, the longer NW network can endure the larger strain due to the remarkable stress relaxation resulting from the high degree of freedom for deformation and the minimal mechanical deterioration of sparse junctions. Figure 2b is a cross-sectional TEM image of the junction of two AgNWs which were well-welded and fused like a single body by the thermal annealing process. During the nanowelding phenomenon, the width of AgNWs can be slightly spread and enlarged by the heat-induced fusing effect, as shown in Figure 2b and the inset. The long-shaped and well-connected nanostructure of the VLNP network efficiently accommodates mechanical deformation with no significant mechanical breakage or electrical degradation, compared to conventional metal thin films which can be easily ruptured into fragments under equivalent stretching deformation.

Figure 2c shows the relative resistance changes during stretching deformation depending on the AgNW length: a short AgNW (top panel, average length of 3 μm and maximum length of 5 μm) electrode, a medium AgNW (middle panel, average length of 20 μm and maximum length of 50 μm) electrode, and the very long AgNW percolated electrode. The VLNP electrode on the PEC exhibited highly stable electrical and mechanical properties under large strain, compared to short AgNW and medium AgNW electrodes, as predicted by the FEA simulations. The short AgNW network electrode showed a drastic resistance upsurge due to deformation-induced fracture. Additionally, the short AgNWs did not transfer well onto the PEC (Supporting Information, Figure S4) mainly because they easily got stuck into the Teflon filter during the suction pressure process. The medium AgNW network electrode had somewhat better properties than the short NW electrode, but still not enough for super-stretchability. This result proved the advantages of VAgNWs for ultra-stretchable electronic and energy devices, including stable reversibility as well as outstanding elasticity. In addition, the sheet resistance of the annealed electrode was evaluated at various elongation strains of PEC, compared to the non-annealed one, as plotted in Figure 2d. The low resistance of thermally nanowelded VLNP electrode on the PEC was retained at highly stretching strain without mechanical damage, whereas the non-annealed sample showed high initial resistance and rapid conductivity degradation with serious delamination even upon mild elongation. The aforementioned property of VLNP on the PEC is ascribed to the fact that the nanowelding preserves the entire percolation network structure under high strain, because the well-fused junctions between the VAgNWs are able to endure the mechanical stress without significant junction disconnection, as shown in the inset of Figure 2d. Moreover, the percolated NW network can be partially sunken down into the silicone-rubber substrate during the thermal annealing process due to the reptation behavior of

ADVANCED MATERIALS
www.advmat.de

www.MaterialsViews.com

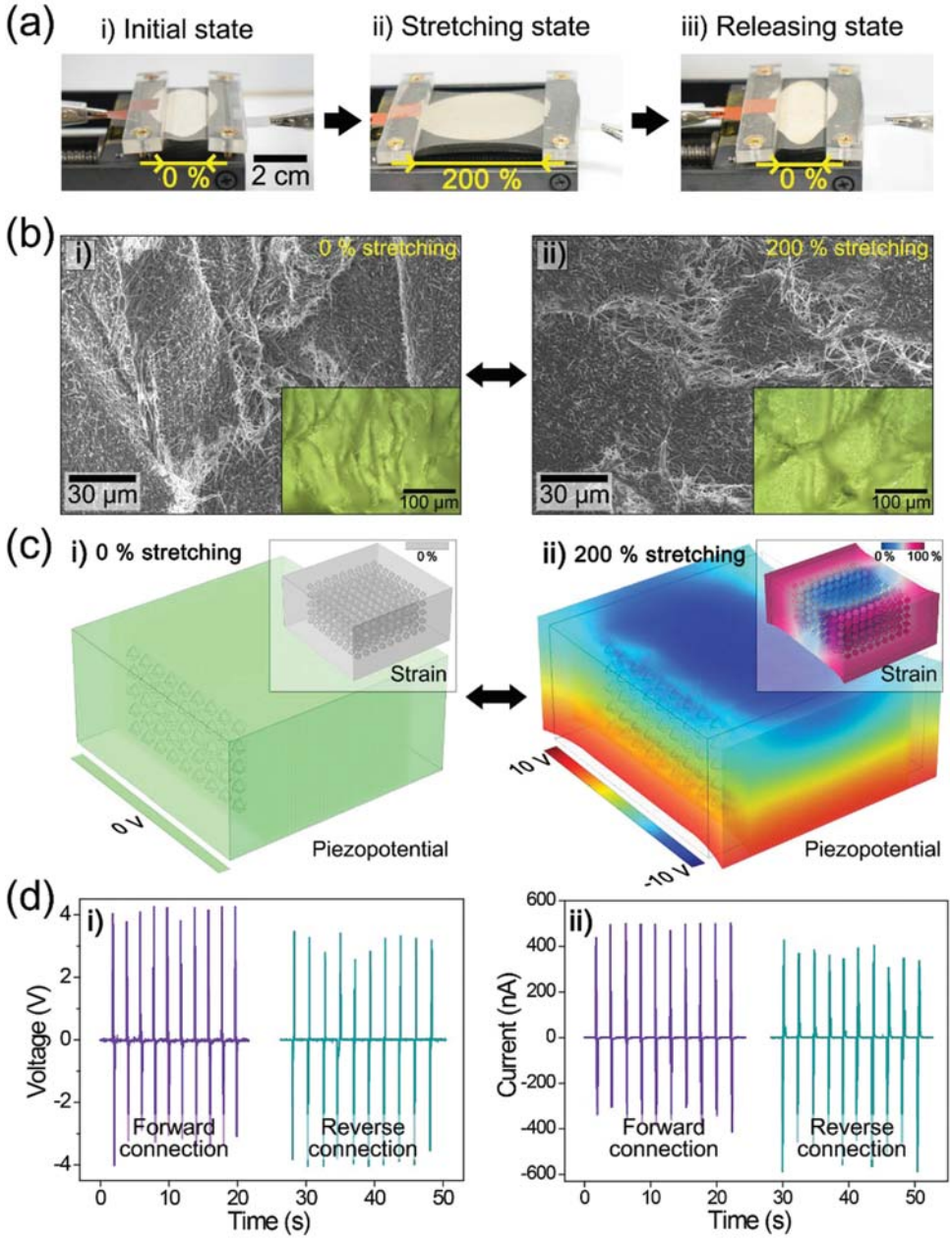

Figure 3. a) Photographs of the SEG device in original, stretching, and releasing states for energy harvesting. b) Microscopic behavior of the VLNP electrodes with: i) releasing (0% stretching) state and ii) 200% stretching state, which are shown by SEM and OM (inset) images. c) 3D FEA simulation using COMSOL multiphysics software to investigate the mechanical energy harvesting of SEG in stretching motions. Piezopotential and strain (inset) are depicted by color codes, when released (i) and stretched (ii). d) During the periodical stretching/releasing deformations, the generated output open-circuit voltage (i) and short-circuit current (ii) from the SEG device in the forward and reverse connections with measuring equipment (switching polarity).

the elastomer (Supporting Information, Figure S5), which can help fix the VLNP shape under stretching conditions. On the contrary, the non-annealed NW patch on the PEC was easily delaminated and deteriorated under tensile force, owing to the absence of the welding and sinking effect, as demonstrated in Figure 2d.

Periodic stretching/releasing tests of the SEG were performed using a linear motor with acyclic motion to apply a strain of 200% at strain rate of 1300% s^{-1} and frequency of 0.5 Hz to measure electrical output from the stretchable energy harvester. **Figure 3**a displays three states of the SEG with the linear motor machine, i.e., initial, stretching, and releasing states. To further confirm the mechanical stability of stretchable VLNP electrodes, we investigated the morphologies of the percolated VAgNWs at both releasing and stretching states using SEM and optical microscopy (OM), as shown in Figure 3b. The set of images (left-hand side at 0% stretch, right-hand side at 200% stretch) strongly validates that the morphological features of the

percolated VAgNWs were robustly maintained before and after stretching motions. When the stretching strain was applied, the VLNP network structures simultaneously began to be deformed by aligning to the strain direction.[40,52] The high electrical conductivity of the VLNP electrodes did not significantly decline after stretching, indicating notable stability under the large elongation of 200%. An FEA simulation was conducted to examine the generated piezoelectric potential distribution in the stretched SEG, as shown in Figure 3c. When the stretchable PEC is exposed to stretching deformation, tensile stress arises along the strain direction, which concurrently provokes compressive stress in the perpendicular directions because of Poisson's effect (insets of Figure 3c). Figure 3c(ii) shows the color-coded piezopotential differences inside the PEC between the top and bottom VLNP electrodes. The calculated piezoelectric potential for a tensile stress of 200% in the silicone elastomer is built up across the elastic composite by the piezoelectric particles. In contrast, poorly dispersed PEC without MWCNT dispersing agents cannot provide the well-distributed piezoelectric potential, as simulated in Figure S6 in the Supporting Information.

To measure the output open-circuit voltage and short-circuit current from the SEG, we used a source-meter (Keithley 2612A), a linear motor controller, a bespoke motion platform, and a voltage follower circuit with high impedance in a grounded Faraday cage to exclude extraneous noise effects. Figure 3d presents the typical electrical output of the stretchable piezoelectric energy harvester under forward and reverse connection with the measurement equipment. The generated voltage (Figure 3d(i)) and current (Figure 3d(ii)) of the SEG when harnessing 200% stretching motion reached up to ≈4 V and ≈500 nA, which are about ten and seven times higher stretchability and output power signals, compared to the previously reported stretchable nanogenerator. It is well known that applying high stretching strain to mechanically robust piezoelectric components can result in outstanding piezoelectric responses due to the enhanced variation of dipole moments, thus improving the generated output power. A polarity switching test using the opposite connections was conducted to demonstrate the reversal of signal peaks, to prove that the generated output by the SEG was purely introduced by piezoelectricity. The deviation of experimental data from the simulated output value is probably due to discrepancies in the actual VLNP coverage, circuital/instrumental impedance, and dynamic mechanics. The amplitude of the output signals produced from the SEG depends upon the composition of the PEC and the presence of CNTs (Supporting Information, Figure S7 and S8), as well as the degree of stretching strain (Supporting Information, Figure S9). The stretching strain of the VLNP electrode itself was not limited at 200%, but the glide of fixture clamps and the mechanical failure of rigid wiring solder (Supporting Information, Figure S10b) caused measurement breakdown.[40] We suggest that using newly designed clamps and soft solders[53] to endure more strain than 200% will be more effective in scrutinizing the relationship between ultra-stretchability (>200%) and corresponding electric output. The generated voltage and current were almost the same under different stretching frequencies (Supporting Information, Figure S11), which indicates that the SEG would be capable of scavenging energy from irregular stretching agitations.

In addition, it was found that the piezoelectric components were readily stimulated and activated by diverse kinds of mechanical stresses such as twisting, folding, and crumpling. To the best of our knowledge, this unusual harnessing is the first demonstration of direct electricity generation beyond simple stretchability for a highly elastic deformable piezoelectric energy harvester. **Figure 4**a–c shows twisting, folding, and crumpling of the SEG without any mechanical failure, respectively. Under the diverse deformations, the VLNP electrodes were neither destroyed nor scarred, as shown in Figure S10a in the Supporting Information. The SEG can generate voltage (Figure 4d) and current (Figure 4e) with the manifold mechanical stimuli. Note that the produced electricity was measured to be smaller than that of the stretching case because the degree of ferroelectric dipole rearrangement may vary with the kind of deformation (e.g., real applied strain, multi-directional stress, etc.). The capability of energy harvesting by alternative stretching motions between the deformations also remained, as presented in Figure 4d,e. The changes of resistance of VLNP under these deformations were also measured to evaluate the robustness of VLNP, as shown in Figure S12 in the Supporting Information. The VLNP is relatively stable during and after various mechanical stimuli. The lowest peaks of folding case are presumably due to the increasing resistance of convexly folded VLNP and the narrowly deformed region compared to other deformations. Electrical signals also appeared when the SEG was pressed, as shown in Video S1 in the Supporting Information. The outstanding elasticity, stretchability, and deformability of the SEG is mainly attributed to the monolithic assembly between the PEC and VLNP electrodes, in contrast to previous nanocomposite generators including two stiff plastic/metal substrates. Furthermore, the enhanced bendability or pressability afforded by the silicone rubbery PEC can lead to improved output performance, compared to conventional PDMS or PVDF-based composite piezo-generators. This stretchy-mechanical compliance of the SEG would also allow energy harvesting from transportation systems pertaining to automobile spring-based suspensions of seats and frames (Supporting Information, Figure S13).

The poling process is basically derived from the principle that most of the piezoelectric dipoles are aligned parallel to the direction of the external electric field and stabilized as remnant polarization to intensify the piezoelectric effect. **Figure 5**a shows the range of voltage and current signals produced from the SEG when polarized at varied levels of applied poling voltage from 0 to 50 kV cm^{-1}. The electrical output of a non-poled SEG gradually increased up to about 4 V and 500 nA as the poling electric field increased by 50 kV cm^{-1}. The inset of Figure 5a shows that the output voltage of the SEG was measured to be consistent, without significant degradation, during about 15 000 repeated stretching motions. This means that our stretchable VLNP electrodes and rubber-based SEG exhibited proper reversible mechanical and electrical characteristics under reciprocating 200% deformation. This result is the best reported performance amid currently developed stretchable nanogenerators. Since the output response of a piezoelectric generator is affected by strain rate, the faster rate caused higher

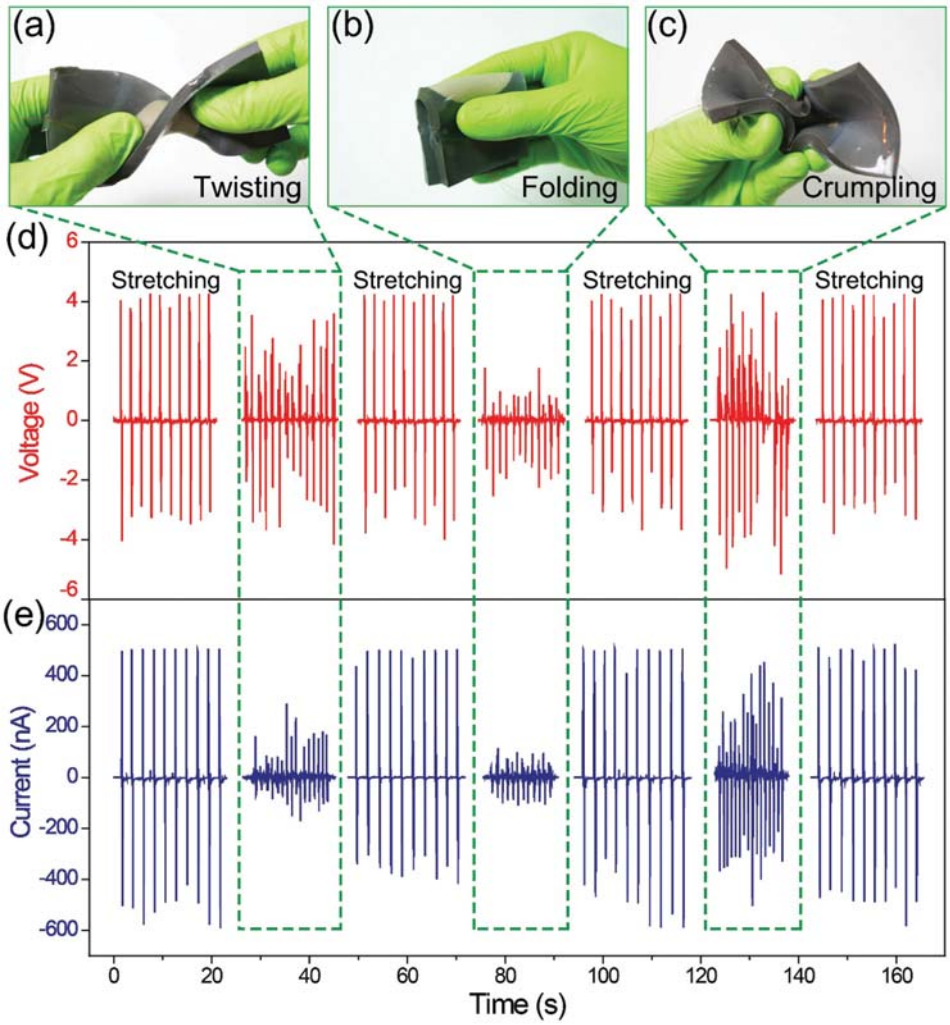

Figure 4. a–c) Photographs of the SEG when subjected to various deformations, such as twisting, folding, and crumpling, which can be converted into corresponding electricity: d) voltage and e) current. These energy-harvesting properties are also shown in Video S1 in the Supporting Information.

output signals from the SEG at the constant stretching strain, as shown in Figure 5b.

The output electric power generated by the stretched SEG was sufficient to operate commercial electronic units. Figure 5c presents a liquid-crystal display (LCD) screen directly driven by the generated output electricity while the SEG was being stretched. The LCD screen was continuously powered by the stretching and releasing deformation of the SEG (Supporting Information, Video S1). Furthermore, three 1 mF capacitors in parallel were utilized to store the electrical potential from the stretched SEG with a bridge rectifier (right inset of Figure 5d). The charged voltage of ≈1.6 V was made available at each capacitor by the continual stretching/releasing deformation of the SEG for ≈2 h (2 Hz). As displayed in the left inset of Figure 5d, the total stored potential of the three capacitors in series reached up to about 4.7 V. Consequently, an amber light-emitting diode (LED) bulb was successfully turned on by the stored electrical energy (Figure 5d and Video S1 in the Supporting Information). These results confirm the ability to operate commercial electronic devices using the stretchable piezoelectric energy harvester. The SEG was then sewn onto the knee of a nylon stocking to emphasize the stretchability and feasibility of our stretchable energy harvester for wearable systems (Figure 5e). Although biological motions are typically expected to be elongated with about 5–30% strain, real stretchable energy systems in wearable/biomedical electronics are required to stretch over hundreds percent for protection against active device failure with strain-compatible integration and prolonged stable operation with mechanical margin.[8–10,54–56] The upper panel of Figure 5e shows the intentionally stretched SEG stitched onto the stocking with a strain of ≈80% diagonally. The attached SEG was also worn over a human thigh, inducing an elongation of about 40% (lower panel of Figure 5e). Moreover, when sewn over a human knee, the SEG could be stretched up to approximately 50%, and produced voltage/current (0.7 V and 50 nA) as a result of the biomechanical stretching motions of kneeling and releasing movement, as presented in Figure 5f.

In conclusion, we have realized a hyper-stretchable elastic-composite generator (SEG) comprised of VLNP network electrodes and PEC. The SEG, consisting of well-dispersed PMN-PT

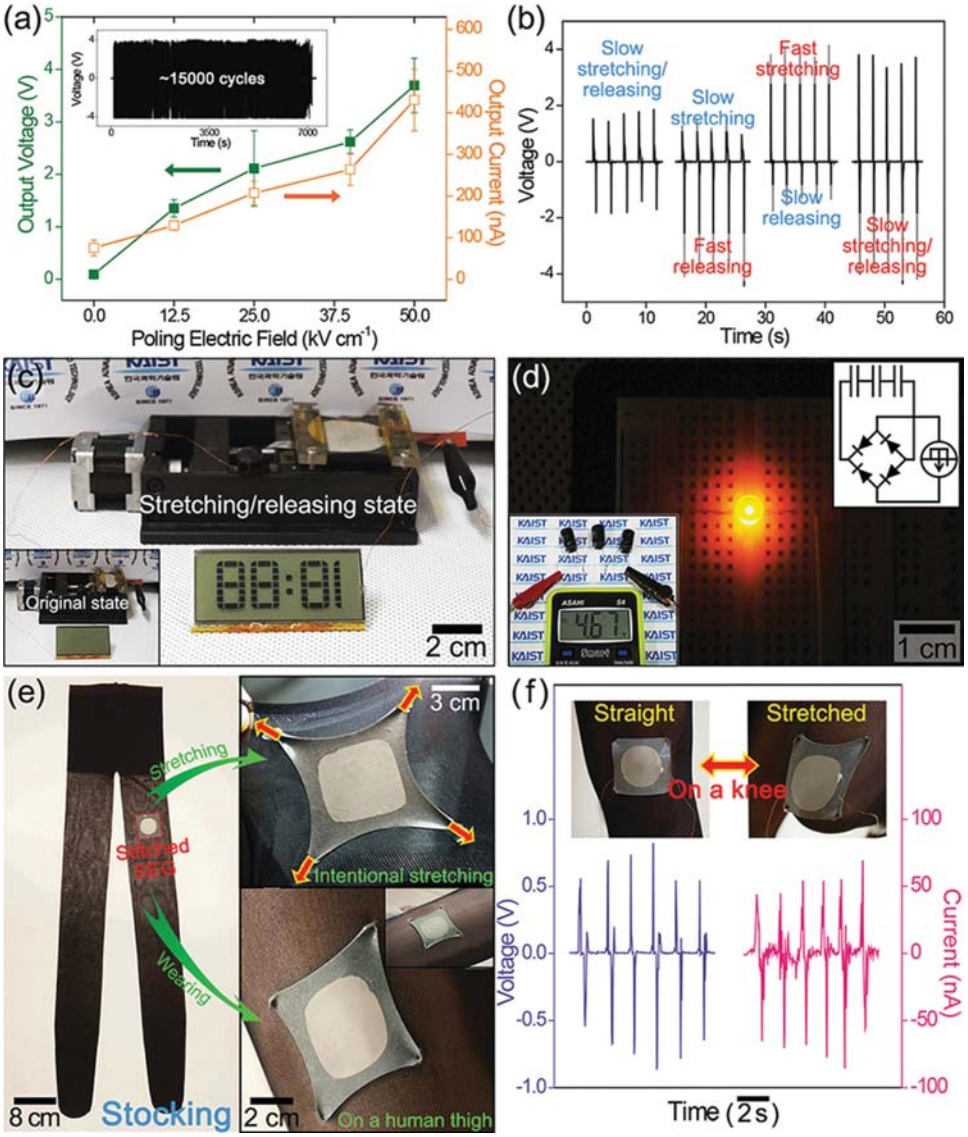

Figure 5. a) Output voltage and current produced by the stretched SEG device as a function of poling electric field. Inset is the durability test of the SEG. b) Voltage signals generated by the SEG in accordance with different strain rates (0.4 vs 0.13 m s^{-1}). c) The commercial LCD screen operated by electrical energy provided from stretching/releasing deformation of the SEG. d) A captured photograph showing a commercial amber LED bulb lighted by the stored potential in capacitors (bottom inset) which are charged by the electrical energy generated from the SEG device. The top inset depicts the rectifying and capacitor charging circuit with the stretchable and deformable energy harvester. This commercial feasibility is also presented in Video S1 in the Supporting Information. e) Photographs of the SEG stitched on a nylon stocking. It can be intentionally stretched (upper right panel) and fitted on a lady's thigh (lower right panel). f) The generated voltage and current from the SEG on the stocking by bending and straightening the knee.

microparticles and MWCNTs with a silicone-rubber matrix, generated outstanding electrical output (≈4 V and ≈500 nA) with a stretchability of 200%. The remarkable elastic responses of the PEC to the large strain guaranteed a high degree of piezoelectricity, induced by the effective rearrangement of dipoles, thus resulting in high-performance energy harvesting. Moreover, the hyper-stretchability of the VLNP-based device was established by VAgNWs which enabled a large degree of freedom to deformation and non-destructive stress relaxation without electrical degradation. The potential generating capability of PEC and the strain capacity of VLNP were confirmed by numerical FEA simulations, subject to the above sophisticated phenomenological mechanisms. Various mechanical deformations (e.g., twisting, folding, and crumpling) as well as stretching motion of the SEG could directly lead to the output voltage and current with mechanical and electrical robustness. The developed SEG also showed practical feasibility for driving commercial electronic units and mounting on the wearable clothes, in contrast with previous reports. This highly elastic piezoelectric generator with stretchability up to 300% and robust energy conversion could open an avenue to the new platform for extensible microelectromechanical systems (MEMS),[57] triboelectric applications,[58,59] universal wearable devices,[60] and self-powered stretchable electronics. We are currently making efforts for

ADVANCED MATERIALS
www.advmat.de

www.MaterialsViews.com

energy-harvesting systems in automobile suspensions, shock absorbers, and tires using this technology to achieve the critical requirements of practical consumer applications.

Supporting Information

Supporting Information is available from the Wiley Online Library or from the author.

Acknowledgements

C.K.J. and J.L. contributed equally to this work. This work was supported by National Research Foundation (NRF) of Korea (Grant No. NRF-2014R1A2A1A12067558 and 2012–0008779), as well as Global Frontier R&D Program on Center for Integrated Smart Sensors (Grant No. CISS-2012M3A6A6054193), and on Center for Multiscale Energy System (Grant No. 2012–054172) funded by Ministry of Science, ICT, Future Planning (MSIP) through NRF in Korea government. The authors would also like to acknowledge S. Jang and J. H. Han for their support with photography.

Received: January 23, 2015
Revised: February 26, 2015
Published online: March 30, 2015

[1] M. Kaltenbrunner, T. Sekitani, J. Reeder, T. Yokota, K. Kuribara, T. Tokuhara, M. Drack, R. Schwodiauer, I. Graz, S. Bauer-Gogonea, S. Bauer, T. Someya, *Nature* **2013**, *499*, 458.
[2] J. Y. Sun, C. Keplinger, G. M. Whitesides, Z. Suo, *Adv. Mater.* **2014**, *26*, 7608.
[3] S. Park, H. Kim, M. Vosgueritchian, S. Cheon, H. Kim, J. H. Koo, T. R. Kim, S. Lee, G. Schwartz, H. Chang, Z. Bao, *Adv. Mater.* **2014**, *26*, 7324.
[4] J. Kim, M. Lee, H. J. Shim, R. Ghaffari, H. R. Cho, D. Son, Y. H. Jung, M. Soh, C. Choi, S. Jung, K. Chu, D. Jeon, S. T. Lee, J. H. Kim, S. H. Choi, T. Hyeon, D. H. Kim, *Nat. Commun.* **2014**, *5*, 5747.
[5] D. H. Kim, N. Lu, R. Ma, Y. S. Kim, R. H. Kim, S. Wang, J. Wu, S. M. Won, H. Tao, A. Islam, K. J. Yu, T. I. Kim, R. Chowdhury, M. Ying, L. Xu, M. Li, H. J. Chung, H. Keum, M. McCormick, P. Liu, Y. W. Zhang, F. G. Omenetto, Y. Huang, T. Coleman, J. A. Rogers, *Science* **2011**, *333*, 838.
[6] D. H. Kim, N. Lu, R. Ghaffari, Y. S. Kim, S. P. Lee, L. Xu, J. Wu, R. H. Kim, J. Song, Z. Liu, J. Viventi, B. de Graff, B. Elolampi, M. Mansour, M. J. Slepian, S. Hwang, J. D. Moss, S. M. Won, Y. Huang, B. Litt, J. A. Rogers, *Nat. Mater.* **2011**, *10*, 316.
[7] I. Jung, J. Xiao, V. Malyarchuk, C. Lu, M. Li, Z. Liu, J. Yoon, Y. Huang, J. A. Rogers, *Proc. Natl. Acad. Sci. USA* **2011**, *108*, 1788.
[8] S. Xu, Y. Zhang, L. Jia, K. E. Mathewson, K. I. Jang, J. Kim, H. Fu, X. Huang, P. Chava, R. Wang, S. Bhole, L. Wang, Y. J. Na, Y. Guan, M. Flavin, Z. Han, Y. Huang, J. A. Rogers, *Science* **2014**, *344*, 70.
[9] J. A. Rogers, T. Someya, Y. Huang, *Science* **2010**, *327*, 1603.
[10] S. Xu, Y. H. Zhang, J. Cho, J. Lee, X. Huang, L. Jia, J. A. Fan, Y. W. Su, J. Su, H. G. Zhang, H. Y. Cheng, B. W. Lu, C. J. Yu, C. Chuang, T. I. Kim, T. Song, K. Shigeta, S. Kang, C. Dagdeviren, I. Petrov, P. V. Braun, Y. G. Huang, U. Paik, J. A. Rogers, *Nat. Commun.* **2013**, *4*, 1543.
[11] W. Weng, S. Qian, Y. Zhang, S. He, Q. Wu, J. Deng, X. Fang, G. Guan, J. Ren, H. Peng, *Adv. Mater.* **2015**, *27*, 1363.
[12] Z. L. Wang, W. Wu, *Angew. Chem. Int. Ed.* **2012**, *51*, 11700.
[13] S. Y. Chung, S. Kim, J. H. Lee, K. Kim, S. W. Kim, C. Y. Kang, S. J. Yoon, Y. S. Kim, *Adv. Mater.* **2012**, *24*, 6022.
[14] X. D. Wang, *Nano Energy* **2012**, *1*, 13.
[15] C. F. Pan, Z. T. Li, W. X. Guo, J. Zhu, Z. L. Wang, *Angew. Chem. Int. Ed.* **2011**, *50*, 11192.
[16] C. R. Bowen, H. A. Kim, P. M. Weaver, S. Dunn, *Energy Environ. Sci.* **2014**, *7*, 25.
[17] J. Briscoe, S. Dunn, *Nano Energy* **2015**, DOI: 10.1016/j.nanoen.2014.11.059.
[18] K. I. Park, S. Xu, Y. Liu, G. T. Hwang, S. J. Kang, Z. L. Wang, K. J. Lee, *Nano Lett.* **2010**, *10*, 4939.
[19] C. Dagdeviren, B. D. Yang, Y. Su, P. L. Tran, P. Joe, E. Anderson, J. Xia, V. Doraiswamy, B. Dehdashti, X. Feng, B. Lu, R. Poston, Z. Khalpey, R. Ghaffari, Y. Huang, M. J. Slepian, J. A. Rogers, *Proc. Natl. Acad. Sci. USA* **2014**, *111*, 1927.
[20] K. I. Park, J. H. Son, G. T. Hwang, C. K. Jeong, J. Ryu, M. Koo, I. Choi, S. H. Lee, M. Byun, Z. L. Wang, K. J. Lee, *Adv. Mater.* **2014**, *26*, 2514.
[21] G. T. Hwang, H. Park, J. H. Lee, S. Oh, K. I. Park, M. Byun, H. Park, G. Ahn, C. K. Jeong, K. No, H. Kwon, S. G. Lee, B. Joung, K. J. Lee, *Adv. Mater.* **2014**, *26*, 4880.
[22] C. K. Jeong, K. I. Park, J. H. Son, G. T. Hwang, S. H. Lee, D. Y. Park, H. E. Lee, H. K. Lee, M. Byun, K. J. Lee, *Energy Environ. Sci.* **2014**, *7*, 4035.
[23] S. H. Lee, C. K. Jeong, G. T. Hwang, K. J. Lee, *Nano Energy* **2014**, DOI: 10.1016/j.nanoen.2014.12.003.
[24] H. Zhang, X. S. Zhang, X. Cheng, Y. Liu, M. Han, X. Xue, S. Wang, F. Yang, S. A. Shankaregowda, H. Zhang, Z. Xu, *Nano Energy* **2015**, *12*, 296.
[25] H. S. Lee, J. Chung, G. T. Hwang, C. K. Jeong, Y. Jung, J. H. Kwak, H. Kang, M. Byun, W. D. Kim, S. Hur, S. H. Oh, K. J. Lee, *Adv. Funct. Mater.* **2014**, *24*, 6914.
[26] G. T. Hwang, M. Byun, C. K. Jeong, K. J. Lee, *Adv. Healthcare Mater.* **2014**, DOI: 10.1002/adhm.201400642.
[27] K. I. Park, M. Lee, Y. Liu, S. Moon, G. T. Hwang, G. Zhu, J. E. Kim, S. O. Kim, D. K. Kim, Z. L. Wang, K. J. Lee, *Adv. Mater.* **2012**, *24*, 2999.
[28] K. I. Park, C. K. Jeong, J. Ryu, G. T. Hwang, K. J. Lee, *Adv. Energy Mater.* **2013**, *3*, 1539.
[29] H. Sun, H. Tian, Y. Yang, D. Xie, Y. C. Zhang, X. Liu, S. Ma, H. M. Zhao, T. L. Ren, *Nanoscale* **2013**, *5*, 6117.
[30] C. K. Jeong, K. I. Park, J. Ryu, G. T. Hwang, K. J. Lee, *Adv. Funct. Mater.* **2014**, *24*, 2620.
[31] C. K. Jeong, I. Kim, K. I. Park, M. H. Oh, H. Paik, G. T. Hwang, K. No, Y. S. Nam, K. J. Lee, *ACS Nano* **2013**, *7*, 11016.
[32] Z. Zhou, H. Tang, H. A. Sodano, *Adv. Mater.* **2014**, *26*, 7547.
[33] K. I. Park, S. B. Bae, S. H. Yang, H. I. Lee, K. Lee, S. J. Lee, *Nanoscale* **2014**, *6*, 8962.
[34] T. I. Lee, W. S. Jang, E. Lee, Y. S. Kim, Z. L. Wang, H. K. Baik, J. M. Myoung, *Energy Environ. Sci.* **2014**, *7*, 3994.
[35] J. Chun, N. R. Kang, J. Y. Kim, M. S. Noh, C. Y. Kang, D. Choi, S. W. Kim, Z. L. Wang, J. M. Baik, *Nano Energy* **2015**, *11*, 1.
[36] Y. Qi, J. Kim, T. D. Nguyen, B. Lisko, P. K. Purohit, M. C. McAlpine, *Nano Lett.* **2011**, *11*, 1331.
[37] X. Feng, B. D. Yang, Y. M. Liu, Y. Wang, C. Dagdeviren, Z. J. Liu, A. Carlson, J. Y. Li, Y. G. Huang, J. A. Rogers, *ACS Nano* **2011**, *5*, 3326.
[38] Y. Q. Duan, Y. A. Huang, Z. P. Yin, N. B. Bu, W. T. Dong, *Nanoscale* **2014**, *6*, 3289.
[39] J. H. Lee, K. Y. Lee, M. K. Gupta, T. Y. Kim, D. Y. Lee, J. Oh, C. Ryu, W. J. Yoo, C. Y. Kang, S. J. Yoon, J. B. Yoo, S. W. Kim, *Adv. Mater.* **2014**, *26*, 765.
[40] P. Lee, J. Lee, H. Lee, J. Yeo, S. Hong, K. H. Nam, D. Lee, S. S. Lee, S. H. Ko, *Adv. Mater.* **2012**, *24*, 3326.

[41] J. Kelly, M. Leonard, C. Tantigate, A. Safari, *J. Am. Ceram. Soc.* **1997**, *80*, 957.
[42] E. B. Araujo, R. N. Reis, C. A. Guarany, C. T. Meneses, J. M. Sasaki, A. G. Souza, J. Mendes, *Mater. Chem. Phys.* **2007**, *104*, 40.
[43] D. Viehland, A. Amin, J. F. Li, *Appl. Phys. Lett.* **2001**, *79*, 1006.
[44] N. N. Wu, Y. D. Hou, C. Wang, M. K. Zhu, X. M. Song, H. Yan, *J. Appl. Phys.* **2009**, *105*, 084107.
[45] D. S. Hecht, L. B. Hu, G. Irvin, *Adv. Mater.* **2011**, *23*, 1482.
[46] A. Kumar, C. W. Zhou, *ACS Nano* **2010**, *4*, 11.
[47] K. E. Korte, S. E. Skrabalak, Y. N. Xia, *J. Mater. Chem.* **2008**, *18*, 437.
[48] J. H. Lee, P. Lee, D. Lee, S. S. Lee, S. H. Ko, *Cryst. Growth Des.* **2012**, *12*, 5598.
[49] J. Lee, P. Lee, H. B. Lee, S. Hong, I. Lee, J. Yeo, S. S. Lee, T. S. Kim, D. Lee, S. H. Ko, *Adv. Funct. Mater.* **2013**, *23*, 4171.
[50] A. M. Leach, M. McDowell, K. Gall, *Adv. Funct. Mater.* **2007**, *17*, 43.
[51] M. T. McDowell, A. M. Leach, K. Gaill, *Nano Lett.* **2008**, *8*, 3613.
[52] Y. Won, A. Kim, W. Yang, S. Jeong, J. Moon, *NPG Asia Mater.* **2014**, *6*, e132.
[53] J. Lessing, S. A. Morin, C. Keplinger, A. S. Tayi, G. M. Whitesides, *Adv. Funct. Mater.* **2015**, *25*, 1418.
[54] J. Lee, J. Wu, M. Shi, J. Yoon, S. I. Park, M. Li, Z. Liu, Y. Huang, J. A. Rogers, *Adv. Mater.* **2011**, *23*, 986.
[55] J. Lee, J. Wu, J. H. Ryu, Z. Liu, M. Meitl, Y. W. Zhang, Y. Huang, J. A. Rogers, *Small* **2012**, *8*, 1851.
[56] T. Someya, *Stretchable Electronics*, Wiley-VCH, Weinheim, Germany **2013**.
[57] A. Koka, H. A. Sodano, *Nat. Commun.* **2013**, *4*, 2682.
[58] C. K. Jeong, K. M. Baek, S. Niu, T. W. Nam, Y. H. Hur, D. Y. Park, G. T. Hwang, M. Byun, Z. L. Wang, Y. S. Jung, K. J. Lee, *Nano Lett.* **2014**, *14*, 7031.
[59] M. Taghavi, V. Mattoli, A. Sadeghi, B. Mazzolai, L. Beccai, *Adv. Energy Mater.* **2014**, *4*, 1400024.
[60] S. Lim, D. Son, J. Kim, Y. B. Lee, J. K. Song, S. Choi, D. J. Lee, J. H. Kim, M. Lee, T. Hyeon, D. H. Kim, *Adv. Funct. Mater.* **2015**, *25*, 375.